Nanocube structured α-Fe_2O_3 films mediated by Ag_3PO_4 for solar water splitting

Chuangli Zhang [a,b], Quanping Wu [a *], Xuebin Ke [c], Jinlin Guo [b], Song Xue [b], Hongyan Wang [b *]

[a] *School of Electric Engineering, Tianjin University of Technology, Tianjin, 300384, China;*

[b] *Tianjin Key Laboratory of Organic Solar Cells and Photochemical Conversion, School of Chemistry & Chemical Engineering, Tianjin University of Technology, Tianjin, 300384, China;*

[c] *School of Engineering, University of Hull, Hull, HU6 7RX, UK*

Corresponding author: Fax: +86-22-60214252; E-mail address: wqping@ustc.edu.cn; wanghongyan12@hotmail.com.

Abstract

A new strategy for surface treatment of hematite nanocubes for efficient photoelectrochemical (PEC) performances is proposed. Silver orthophosphate (Ag_3PO_4) was adopted to mediate the formation of α-Fe_2O_3 films. Phosphate ions in Ag_3PO_4 caused a significant morphology change during annealing process, from β-FeOOH nanorod arrays to hematite nanocubes. Meanwhile, Ag ions were doped into α-Fe_2O_3 film. The obtained nanocube structured Fe_2O_3-Ag-P films demonstrated much higher photoelectrochemical performance as photoanodes than the bare Fe_2O_3 nanorod thin films. The effects of phosphate and silver ions on the morphology, surface characteristics and the PEC properties of the photoanodes are investigated.

Key words: Hematite film; Silver orthophosphate; Photoelectrochemical water splitting; Photocurrent

1. Introduction

Hematite (α-Fe_2O_3) has been considered as an attractive semiconductor material for photoelectrochemical (PEC) water splitting due to its narrow band gap (2.1–2.2 eV),

appropriate chemical stability in alkaline environment, nontoxicity, and low cost [1-4]. A photocurrent of 12.6 mA/cm^2 in water splitting has been predicted under AM 1.5G solar irradiation[5]. At present, the best record of photocurrent as high as 4.32 mA/cm^2 was achieved by Pt-doped α-Fe_2O_3 nanorods coated with Co-Pi cocatalyst at 1.23 V_{RHE}[6]. The inherent obstacles for hematite as photoanode in PEC performances are mainly concerned with the extremely short hole diffusion length (2–4 nm) [7], poor conductivity[8] and slow oxygen evolution reaction kinetics[9]. These features limit charge transport and cause a serious recombination of electrons and holes. Thus increasing surface oxidation reaction kinetics and suppressing charge recombination occurring in the bulk and the surface of α-Fe_2O_3 become the key points for improved PEC performances [10, 11].

Previous reports show that surface modification is one of the successful approaches (e.g. elemental doping, nanostructure morphology) for α-Fe_2O_3 to improve the photocurrent [12-16]. A thin overlayer of metal oxide, such as Al_2O_3, Ga_2O_3 or In_2O_3 could passivate surface states of α-Fe_2O_3 and effectively accelerate solar water oxidation reaction kinetics with a shift of the photocurrent onset potential [17, 18]. The oxidation reaction kinetics can also be improved by surface modification with co-catalysts IrO_2, NiOx and Pi-Co [9, 19-23]. These co-catalysts generally catalyze inert oxygen evolution reaction and suppress surface charge recombination which results in an increased photocurrent. In addition, surface doping of metal ions are being reported to improve the PEC performances of α-Fe_2O_3 [24-26]. Surface treatment with Sn resulted in formation of $Fe_xSn_{1-x}O_4$ at the hematite surface and caused the photocurrent density to increase from 1.24 to 2.25 mA cm^{-2} at 1.23 V_{RHE} [27]. The enhancement was mainly attributed to a reduced surface charge recombination. Similarly, a thin overlayer of $Ni_xFe_{2-x}O_3$ on the surface of hematite nanotubes was found to have accelerated surface oxygen evolution, promoted charge transfer, and resulted in better performances in water splitting relative to the pristine α-Fe_2O_3[28]. Very recently, α-Fe_2O_3/$Ag_xFe_{2-x}O_3$ core shell structured hematite nanorod films were synthesized with a 2–3 nm thick $Ag_xFe_{2-x}O_3$ overlayer covered along the nanorods [11]. The doped Ag effectively increased the charge density in the near-surface of hematite,

and also improved the surface oxidation ability, thus led to enhanced PEC performances. Apart from metal ions, phosphate ions were reported to modify α-Fe_2O_3 by simply immersing hematite film in an aqueous sodium phosphate solution[29]. A negative electrostatic field is formed by the phosphate ions on hematite surface, which promotes extraction of holes to the electrode surface and suppresses surface charge recombination. In our previous study[30], attempts were made to build up the negative electrostatic fields on the surface of hematite films through different approaches: soaking the bare hematite films in Na_2HPO_4 solution or introducing Na_2HPO_4 to the $FeCl_3$ starting solution. It was found that more phosphate ions were coated on the hematite films by latter route, which resulted in the formation of stronger negative electrostatic field. Moreover, the morphology of α-Fe_2O_3 was changed from nanorod to nanocube structure in the presence of the phosphate salt. The as-synthesized hematite demonstrated higher photoelectrochemical performances as photoanodes because of stronger negative electrostatic field and the less bulk recombination due to the nanocube structure.

In this study, silver orthophosphate (Ag_3PO_4) is proposed to mediate the formation of α-Fe_2O_3 from FeOOH via surface treatment. It is found that after annealing, FeOOH nanorods could be converted into α-Fe_2O_3 nanocubes if FeOOH surface was pre-treated with Ag_3PO_4. It is revealed that Ag doping and phosphate modification have greatly improved PEC performances of hematite and an extremely high hole injection yield (93.8%) was obtained. The effects of phosphate and Ag ions on the morphology, surface characteristics and the PEC properties of the photoanodes are investigated.

2. Experimental section

2.1. Materials preparation

Preparation of β-FeOOH film

β-FeOOH nanorod arrays were grown on fluorine-treated tin oxide (FTO, Nippon Sheet Glass Co. Ltd, 15 ohm/sq, 1×2.5 cm^2) substrate in an aqueous solution as reported by Vayssieres [32]. Typically, a 4 mL aqueous solution containing 6 mmol of $FeCl_3$ (Sigma-Aldrich) was transferred into a 10 mL beaker, and the substrates were placed with the FTO side facing the wall of the beaker at an angle. The beaker was then

transferred into the 100 mL Teflon-lined autoclave. The autoclave was maintained in a regular oven at 100 °C for 6 h under autogenous pressure, before naturally cooled to room temperature. The obtained yellow films of β-FeOOH nanorod arrays were washed with distilled water and dried.

Preparation of hematite films mediated by Ag_3PO_4 particles

Yellow powdered Ag_3PO_4 particles were prepared by the ion-exchange method according to previous report [31]. In a typical process, a 0.003 mol of $AgNO_3$ was dissolved in 30 ml of H_2O, then 30 ml of K_2HPO_4 aqueous solution (0.001 mol) was added drop by drop into the above solution. After thoroughly stirring for 1h, the yellow precipitate was filtrated, and washed with distilled water for three times. Lastly, the resulted yellow powders were dried in air at 70 ^oC overnight. A certain amount of Ag_3PO_4 particles were dispersed in ethanol solution to give a concentration of 1, 5 and 10 mg/mL. The suspension was applied to β-FeOOH film by spin coating at 1,500 rpm for 30 s. After annealing at 700 °C for 1h with a ramping rate of 5°C /min, the hematite films mediated by Ag_3PO_4 powder were obtained. Based on the concentration of Ag_3PO_4 suspension (1, 5 and 10 mg/mL), the samples are referred to as Fe_2O_3-Ag_3PO_4-1, Fe_2O_3-Ag_3PO_4-5 and Fe_2O_3-Ag_3PO_4-10.

Preparation of hematite films mediated by in-situ formed Ag_3PO_4

A more homogenous deposition of Ag_3PO_4 particles on the β-FeOOH nanorod arrays was achieved by an *in situ* precipitation method. In a typical process, a certain amount of Na_2HPO_4 and $AgNO_3$ were dissolved into water to form a mixed solution with 0.25 M Na_2HPO_4 and 2.5 mM $AgNO_3$. Then β-FeOOH film was immersed into the above mixed solution for 1 h. After washing with deionised water, the hematite films were obtained by annealing at 700 °C for 1h, with a ramping rate of 5°C /min. The sample is abbreviated as Fe_2O_3-Ag-P.

2.2. Materials characterisation

The crystalline structures of the samples were characterised by X-ray powder diffraction (XRD) with a Rigaku D/MAX-2500 powder diffractometer (Japan) using Cu Kα radiation (λ = 0.154 18 nm) and an accelerating voltage of 30 kV and emission current of 20 mA. Scanning electron microscopy (SEM) was taken on a JEOL/JSM7500

with an accelerating voltage of 15 kV to characterise the surface morphology and thickness of the films. Ultraviolet-visible (UV-vis) absorption spectra of the samples were obtained using a UV-visible spectrophotometer (Shimadzu, UV-2600), and $BaSO_4$ was used as a reference.

2.3 Photoelectrochemical measurements

Photoelectrochemical measurements were performed using a three-electrode configuration in 1.0 M NaOH (pH 13.6) aqueous solution at a potentiostat (AutoLab-30 potentiostat), with the hematite samples as the working photoanodes, Ag/AgCl(saturated KCl) as the reference electrode, and Pt as the counter electrode. A 1 cm^2 masked-off, sealed area of photoanodes was irradiated with a 300-W xenon lamp. The light power density (100 mW cm^{-2}) at the position of the sample was measured with a power meter (TYD, FSR-2). 1 M NaOH electrolyte or 1 M NaOH with 0.5 M H_2O_2 electrolyte were degassed by purging N_2 gas for 10 min to remove any dissolved O_2 and therefore suppress the reduction of O_2 at the counter electrode. Incident photon conversion efficiency (IPCE) characteristics were measured with a xenon light source (MAX-302, Asahi Spectra Co. Ltd.) coupled with a monochromator (CMS-100, Asahi Spectra Co. Ltd.) from 369 to 730 nm, at a potential of 1.23 V_{RHE}. All potentials were converted to the reversible hydrogen electrode (RHE) scale using the equation $V_{RHE} = V_{Ag/AgCl}$ + 0.1976 V + pH (0.059 V).

3. Results and discussion

3.1. Fabrication and characterisation of nanocube α-Fe_2O_3 film mediated by spin-coating Ag_3PO_4 powder particles

Yellow powdered Ag_3PO_4 particles were synthesized by a simple ion-exchange process. The phase and purity of the sample were characterized by XRD measurement. As shown in Fig. 1, all of the peaks readily indicate the body-centred cubic structure of Ag_3PO_4. The formed particles were about 300 to 400 nm in size from scanning electron microscopy (SEM) images inserted in Fig. 1. The Ag_3PO_4 particles were dispersed in ethanol solution to give a concentration of 1, 5 and 10 mg/mL. The suspension was applied to FeOOH film by spin coating at 1,500 rpm for 30 s. According to the modified

procedure developed by Vayssieres [32], the highly anisotropic FeOOH film was grown on FTO glass from an aqueous $FeCl_3$ solution. Fig. 2a shows a top-view SEM image of the FeOOH surface. The diameter of the FeOOH nanorods varies from 60 to 80 nm while their length is about 292 nm. After spin coating with 1 mg/mL of ethanol suspension of Ag_3PO_4, the FeOOH surface was coated with some Ag_3PO_4 particles in aggregation. When the concentration is increased to 5 mg/mL, more Ag_3PO_4 particles were observed on the surface (Fig. 3b). At a concentration of 10 mg/mL, the FeOOH surface was almost covered with a thick layer of Ag_3PO_4 particle aggregation (Fig. 3c).

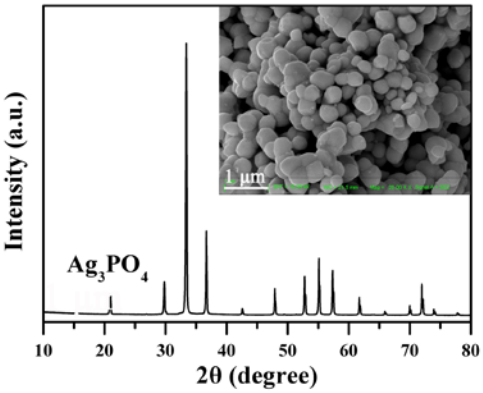

Fig. 1 X-ray diffraction pattern and SEM image (inserted) of Ag_3PO_4.

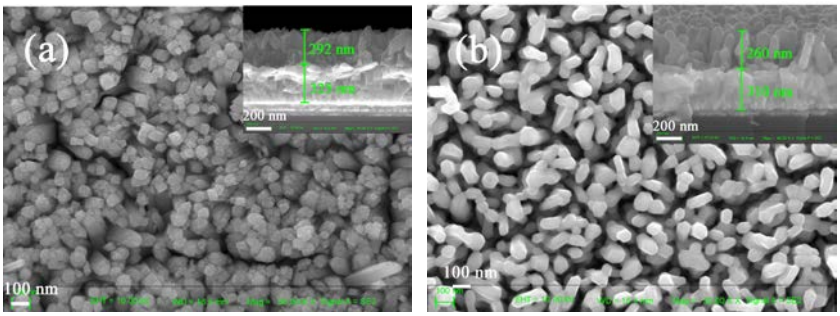

Fig. 2 SEM images of the FeOOH film (a), and bare Fe_2O_3 film (b).

Fig. 3. SEM images of the FeOOH film coated by Ag_3PO_4 powder at concentration of 1 mg/mL (a), 5 mg/mL (b) and 10 mg/mL (c).

These FeOOH thin films were subsequently annealed in air at 700°C for one hour to allow a complete crystal phase conversion to the hematite. As shown in Fig. 2b, the nanorod morphology of bare α-Fe_2O_3 was preserved with little change in the anisotropic dimensions, except for the enlarged feature size and shorter film thickness. In addition, the grain edges of nanorods became smoother. For the sample spin coated

with 1 mg/mL of Ag_3PO_4 suspension, the aggregated Ag_3PO_4 particles couldn't be observed anymore. Instead, some circular areas were observed as shown in Fig.4(b). The image in high magnification reveals that the nanocube structure was formed in the circular areas Fig.4(c). However, outside the circular areas, it was the same nanorod structure as the bare α-Fe_2O_3 (Fig. 4a)。 Therefore, it is clear that the circular areas are the original place covered by Ag_3PO_4 particles. And, the deposited Ag_3PO_4 causes the morphology changes during the conversion of FeOOH to hematite: from nanorod to nanocube structure. When the concentration of Ag_3PO_4 is increased to 5.0 mg/mL, almost the total surface area of α-Fe_2O_3 film had been changed into nanocube morphology, and Ag_3PO_4 particles were not observed on the surface either (Fig. 4 (d) and (e)). The film thickness became shorter in comparison to that of bare α-Fe_2O_3. In the case for higher concentration of Ag_3PO_4 (10 mg/mL), the as-formed nanocube α-Fe_2O_3 film was covered by some pieces of thin films (Fig. 4f). These thin films are probably associated with the excessive Ag_3PO_4 particles located on the surface of FeOOH film, which will be identified by the XRD analysis.

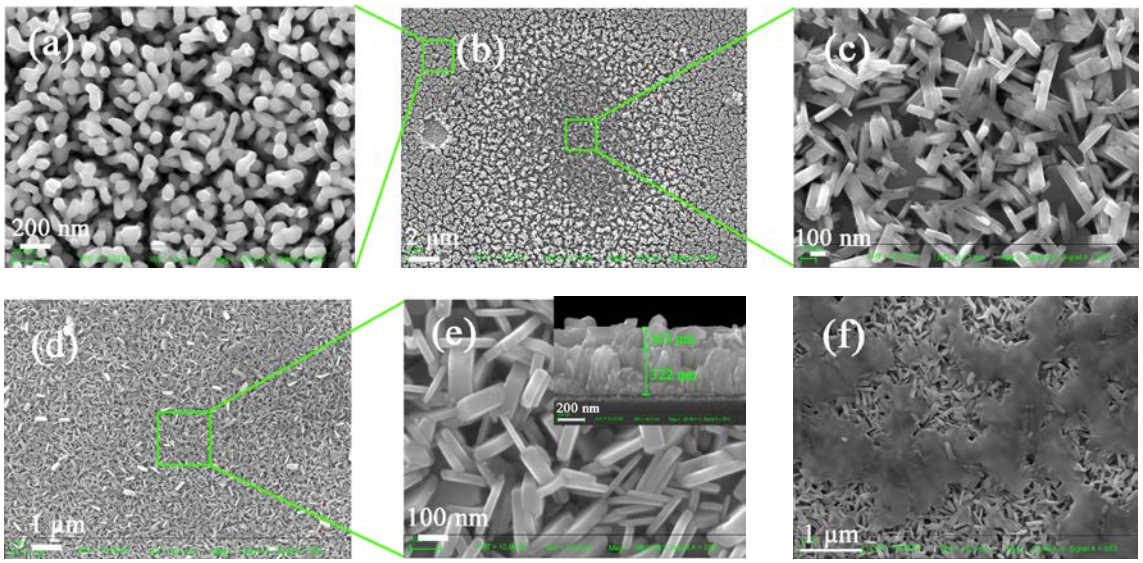

Fig. 4. SEM images of sample Fe_2O_3-Ag_3PO_4-1 (a-c), Fe_2O_3-Ag_3PO_4-5 (d, e), and Fe_2O_3-Ag_3PO_4-10 (f).

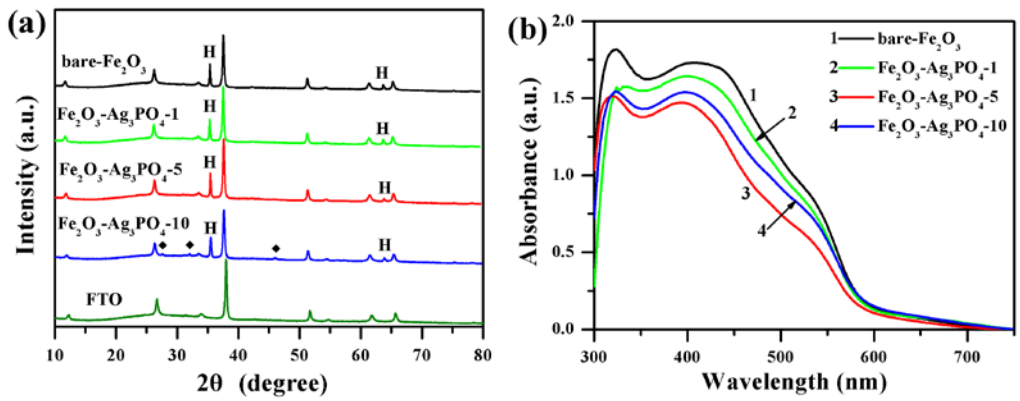

Fig. 5 a) X-ray diffraction pattern of bare Fe_2O_3, Fe_2O_3-Ag_3PO_4-1, Fe_2O_3-Ag_3PO_4-5, and Fe_2O_3-Ag_3PO_4-10; b) UV-vis absorption spectra of the four films.

The three hematite films mediated by Ag_3PO_4 at the concentrations of 1, 5, and 10 mg/mL on FTO were further characterized with XRD analysis. As shown in Fig. 5a, compared with the spectra of FTO substrate, two additional diffraction peaks at 35.8° and 64.2° were clearly observed in all the hematite thin films, which could be assigned to the (110) and (300) planes of α-Fe_2O_3, respectively. At Ag_3PO_4 concentrations of 1 and 5 mg/mL, no other peaks were observed, whereas in the case of a sample at high concentration of 10 mg/mL, three weak diffraction peaks at 27.8 °, 32.3 °, and 46.3 ° could be found, which may be assigned to the presence of silver pyrophosphate ($Ag_4P_2O_7$)[Refences]. So some pieces of thin films located on the surface of α-Fe_2O_3 nanocube in Fig. 4f can be attributed to $Ag_4P_2O_7$. Figure 5b shows the UV-vis absorption spectra of the three films. In comparison to the bare Fe_2O_3, the three films modified by Ag_3PO_4 show a decreasing light absorption because of the thinner film thickness. The sample Fe_2O_3-Ag_3PO_4-10 exhibits a stronger absorption than the sample Fe_2O_3-Ag_3PO_4-5, which might be due to the presence of $Ag_4P_2O_7$. Light absorption ends up at about 590 nm, corresponding to a band gap of 2.1 eV for α-Fe_2O_3.

These observations demonstrate that Ag_3PO_4 plays a vital role on the formation of nanocube morphology of α-Fe_2O_3. In our previous report [30], a similar nanocube structured α-Fe_2O_3 film was formed during hydrothermal process in an aqueous solution of $FeCl_3$ and Na_2HPO_4. Phosphate ions were preferentially adsorbed on certain planes of the initial nuclei, and iron ions (or iron oxides units) continued to grow and

aggregate along other planes, resulting in formation of the nanocube structure. An ellipsoid of α-Fe_2O_3 particles was previously reported to be formed in $FeCl_3$ and KH_2PO_4 solution[33]. It was suggested that phosphate groups were adsorbed on surface of the initial hematite nuclei, resulting in ellipsoidal primary particles with varying prolateness depending on the phosphate concentration. Due to the net magnetic moment that hematite possesses in the c direction, these primary ellipsoidal particles aggregated along their c-axis to give the final ellipsoidal hematite particles. Therefore, in the current case, it can be inferred that the formation of nanocube structured α-Fe_2O_3 from FeOOH nanorods was probably mediated by phosphate ions in Ag_3PO_4 during annealing.

It is well known that H_2O will be produced during the conversion of FeOOH to α-Fe_2O_3. The generated water can dissolve a fraction of Ag_3PO_4 particles at annealing condition. Phosphate ions in the dissolved Ag_3PO_4 would be absorbed on certain planes of the crystal nuclei of iron oxides when FeOOH was converted to α-Fe_2O_3. The final morphological changes from FeOOH nanorods to α-Fe_2O_3 nanocubes were made by crystal growth along another plane in accordance with previous reports. At the same time, Ag^+ in the Ag_3PO_4 could diffuse along the α-Fe_2O_3 nanocube surface and modify the α-Fe_2O_3 by doping. The molar ratios of Ag/Fe and P/Fe for sample Fe_2O_3-Ag_3PO_4-5 detected by EDS were found to be 0.82% and 0.24%, respectively.

Since Ag_3PO_4 was not present on the film surface from SEM and XRD analysis after annealing, it can be inferred that the detected Ag and P elements originated from Ag-doped Fe_2O_3 layer and phosphate modified surface, respectively. In this case, Ag-doped α-Fe_2O_3 nanocubes were simply synthesized from the conversion of FeOOH nanorods in the presence of Ag_3PO_4 powder in the solid phase. Ag doped overlayer of α-Fe_2O_3 nanorod was reported to give improved PEC performances through the increased charge carrier density and the enhanced surface oxidation reaction [11]. Therefore, the Ag-doped α-Fe_2O_3 nanocubes via solid-phase synthesis will be predicted to be effective in PEC water splitting. Furthermore, phosphate ions absorbed on the surface of α-Fe_2O_3 nanocubes will build up a negative electrostatic field, which can promote charge separation and extraction of holes to the electrode surface, resulting in

minimizing surface charge recombination [29, 30]. A schematic diagram for conversion of FeOOH nanorods to α-Fe_2O_3 nanocubes mediated by Ag_3PO_4 was shown in Fig. 6.

At a low concentration of Ag_3PO_4 suspension, such as 1 or 5 mg/mL, silver cations in Ag_3PO_4 were doped into α-Fe_2O_3 nanocubes and phosphate anions were absorbed on nanocube surfaces. Thus Ag_3PO_4 could not be detected on the hematite film. However, there is a limit for Ag doping and phosphate adsorption on the hematite surface. Shen et al described a similar phenomenon that a thin overlayer of $Ag_xFe_{2-x}O_3$ with a limited thickness (2-3 nm) was formed on α-Fe_2O_3 nanorods when Ag precursor solution increased from 0.005 M to 0.1M [11]. In our case, for high Ag_3PO_4 concentration (10 mg/mL), the residual Ag_3PO_4 was converted to $Ag_4P_2O_7$ under annealing conditions. (Fig.5(a)). As shown in Scheme 1, HPO_4^{2-} is generated from PO_4^{3-} by a proton exchange with FeOOH. Two HPO_4^{2-} produce $P_2O_7^{4-}$ through a condensation reaction with an elimination of H_2O. Thus the formed $Ag_4P_2O_7$ film was covered on the surface of the hematite in the case of high concentration of Ag_3PO_4.

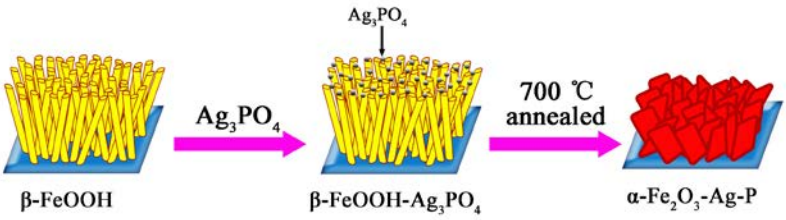

Fig. 6 Conversion of FeOOH nanorods to α-Fe_2O_3 nanocubes mediated by Ag_3PO_4.

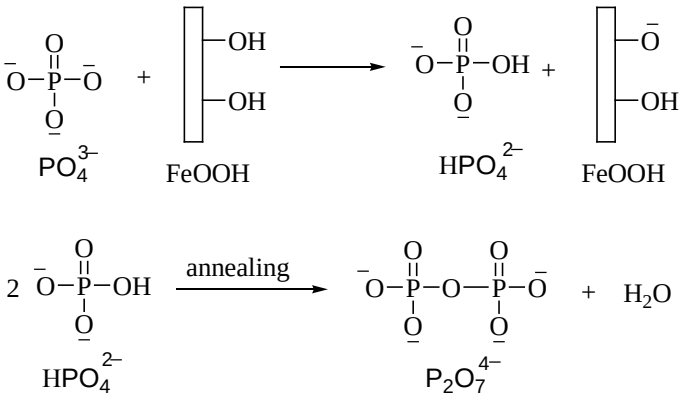

(1)

(2)

Scheme 1. A diagram of PO_4^{3-} converted to $P_2O_7^{4-}$

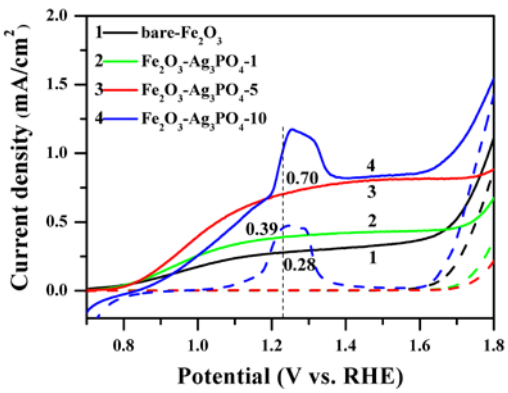

Fig. 7 *J-V* characteristics curves of four films were recorded in 1.0 M NaOH in the dark (dashed lines) and under light illumination (solid lines).

The current-voltage (*J-V*) curves of the as-prepared three hematite films as photoanodes were recorded in the dark and light illumination with 100 mW/cm^2 at the position of all samples. Photocurrent was tested in 1.0 M NaOH (pH=13.6) solution, and the results were shown in Fig. 7. The photocurrents were improved obviously after the hematite films were mediated by Ag_3PO_4. A photocurrent of 0.28 mA cm^{-2} was recorded for the bare Fe_2O_3 at +1.23 V_{RHE}. The photocurrent was improved to 0.39 mA cm^{-2} for Fe_2O_3-Ag_3PO_4-1, and 0.70 mA cm^{-2} for Fe_2O_3-Ag_3PO_4-5 at +1.23 V_{RHE}. The improved photocurrent can be ascribed to the formation of Ag-dpoed α-Fe_2O_3 nanocubes with phosphate adsorbed on the surface. But for Fe_2O_3-Ag_3PO_4-10, a slightly decreased photocurrent was observed at potential below +1.18 V_{RHE} in comparison with the Fe_2O_3-Ag_3PO_4-5. When the potential is higher than +1.18 V_{RHE}, sample Fe_2O_3-Ag_3PO_4-10 showed a steep increase in the photocurrent, followed by a sharp decrease. A similar photocurrent peak was observed in the dark conditions, indicating that it is probably the oxidation peak of Ag+ due to the presence of $Ag_4P_2O_7$ on the hematite surface. It was reported that the oxidation peak was also found in Ag-doped α-Fe_2O_3 nanorod, which was prepared from ultrasonication treatment of FeOOH in aqueous solution of silver acetate. Two kinds of silver ions Ag(I) and Ag(III) were present after *J-V* scan. Part of Ag(I) ions were oxidized to Ag(III) ions at moderate potential, resulting in the oxidation peak [11].

3.2. Synthesis and characterisation of nanocube α-Fe_2O_3 mediated by in-situ formed

Ag_3PO_4

The Ag_3PO_4 powder particles with size in range of 300 to 400 nm were not well dispersed in ethanol solution, and particles coated on the FeOOH surface were observed to be severely aggregated. Aggregation of Ag_3PO_4 particles into larger size is not beneficial to formation of uniform film with well-distributed Ag+ and phosphate ions. To eliminate these unfavorable factors, nano Ag_3PO_4 particles were *in-situ* synthesized through soaking FeOOH in a solution of $AgNO_3$ and KH_2PO_4, which is referred to as Fe_2O_3-Ag-P. Five hematite films were fabricated according to various concentrations of $AgNO_3$ and KH_2PO_4. The *J-V* characterizations of the five films were examined, as shown in Fig. 8. A photocurrent of 0.52 mA cm^{-2} at +1.23 V_{RHE} was obtained in a soaking solution containing 1.0 mM $AgNO_3$ and 0.33 mM KH_2PO_4 (Ag : P molar ratio = 3 : 1). When $AgNO_3$ concentration was increased to 2.5 mM, the photocurrent was improved to 0.66 mA cm^{-2}. The enhanced PEC performance is ascribed to the increasing coverage of Ag_3PO_4 on the soaked FeOOH film. However, further increase in $AgNO_3$ concentration resulted in a decreased photocurrent of the as-synthesized hematite films. For example, the 5.0 mM $AgNO_3$ gave a low photocurrent of 0.26 mA cm^{-2} under the same conditions. In such case with high $AgNO_3$ concentration（5.0 mM）, Ag_3PO_4 particles may have readily precipitated in the solution, not on the FeOOH surface. Thus the concentration of $AgNO_3$ was kept to be 2.5 mM in the following test. When KH_2PO_4 concentration increased to 250 mM, the hematite film exhibited a photocurrent as high as 0.98 mA cm^{-2}, which is higher than that of Fe_2O_3-Ag_3PO_4-5 (0.70 mA cm^{-2}, Fig. 7). These results demonstrate that the *in-situ* formed Ag_3PO_4 in soaking solution is more efficient for enhancement in photocurrent than previous spin-coated Ag_3PO_4 powder.

In order to elucidate the formation process of the Ag_3PO_4 in-situ mediated α-Fe_2O_3 nanocubes, a sample was prepared by soaking FeOOH in a solution of 2.5 mM $AgNO_3$ and 250 mM KH_2PO_4, which was then characterized by XRD analysis. As shown in Fig. 9, compared with the spectra of FeOOH/FTO, one additional diffraction peak at 52.7^o could be observed in the sample, which is assigned to the (222) planes of Ag_3PO_4. This implies that Ag_3PO_4 was generated from the solution of $AgNO_3$ and KH_2PO_4, and

coated on the FeOOH film. After annealing at 700°C for 1h, apart from the peaks at 35.8° and 64.2° for the α-Fe_2O_3, no other peaks, especially at 52.7°, were observed, which suggested that Ag_3PO_4 was not present on the α-Fe_2O_3 film. The sample was further characterized by SEM measurement, as shown in Fig. 10a-b. The formed Ag_3PO_4 was well distributed on the FeOOH film without obvious aggregation. These particles are about 40 to 60 nm in size, which is much smaller than Ag_3PO_4 powder in the samples prepared by spin coating approach. A top-view SEM image in Fig. 10c showed that after annealing, the hematite film was compact and flat. The atomic ratios of P/Fe ($r_{P/Fe}$) and Ag/Fe ($r_{Ag/Fe}$) analyzed by EDS were found to be 0.01and 0.006 respectively. Nanocube morphology was clearly observed with about 178 nm thickness from the side-view SEM image. These observations demonstrate that the *in-situ* formation of Ag_3PO_4 by simple procedure of soaking in solution can mediate conversion of FeOOH nanorods into α-Fe_2O_3 nanocubes, and result in this drastic effect on the photoelectrochemical performance.

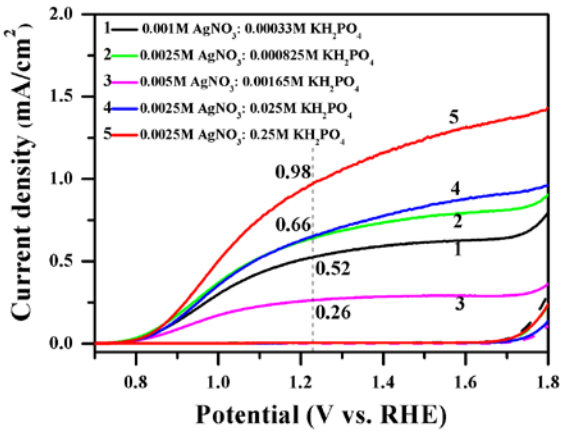

Fig. 8. *J-V* characteristics curves of five films at various concentrations of $AgNO_3$ and KH_2PO_4.

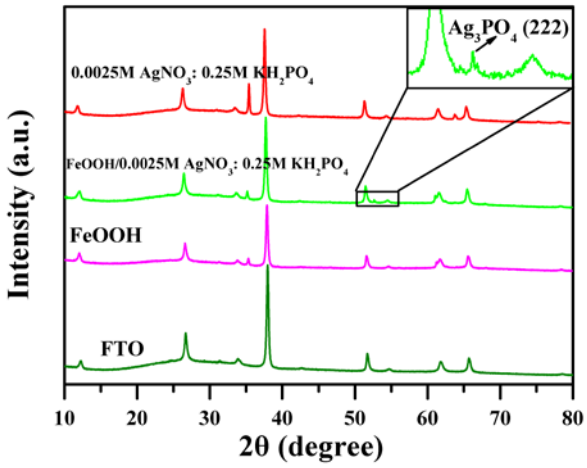

Fig. 9. X-ray diffraction pattern of FeOOH, α-Fe_2O_3 film soaked in solution of $AgNO_3$ and KH_2PO_4.

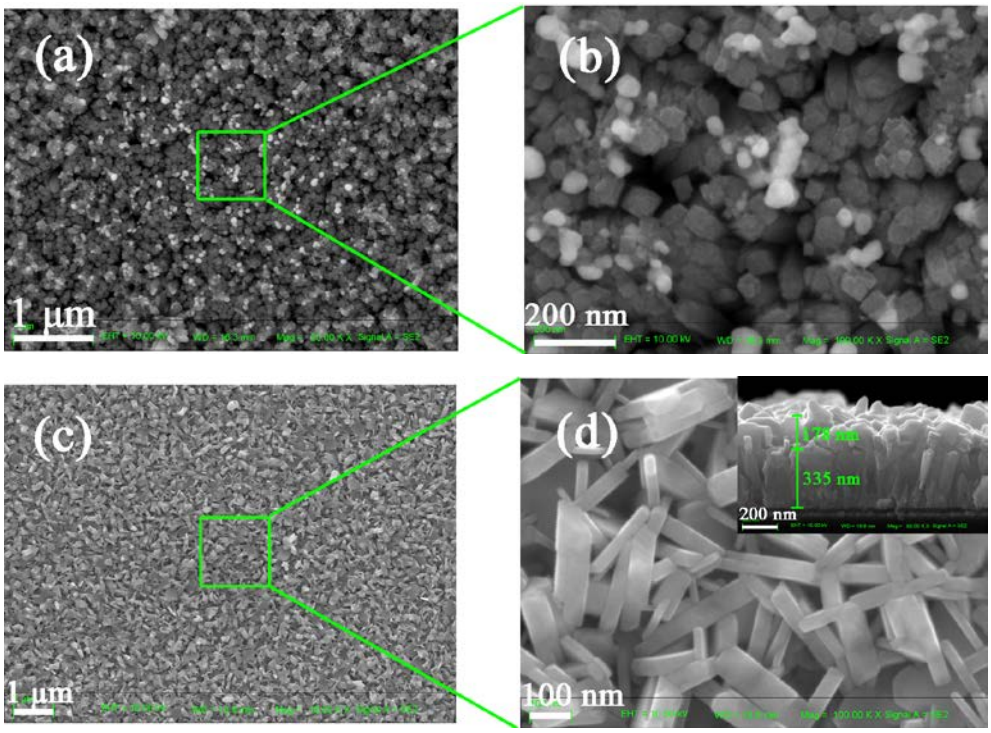

Fig. 10. SEM images of the FeOOH film coating with the Ag_3PO_4 *in-situ* formed from solution of 2.5 mM $AgNO_3$ and 250 mM KH_2PO_4 (a, b), and α-Fe_2O_3 film mediated by the *in-situ* formed Ag_3PO_4 (c, d).

The surface characteristics of Ag-doped α-Fe_2O_3 nanorod films were studied by XPS. In the survey scan of XPS spectra shown in Fig S1, it can be clearly confirmed the presence of Fe, O, P and Ag signals. The fine XPS spectra of Fe 2p (Figure S2) shows Fe2p3/2 and Fe2p1/2 at 711.1 and 724.4 eV respectively, as well as a satellite peak around 719.3 eV. These results are consistent with the characteristics of Fe^{3+} ions in

hematite [34, 35] In the Ag 3d XPS spectra, the peaks of Ag 3d5/2 and Ag 3d3/2 levels are located at ca.367.8 and 374.0 eV respectively (Fig.S2), which are attributed to Ag ions doped in hematite [11, 36, 37]. Also, the high-resolution of P2p spectrum show that the P2p binding energy of 133.0 eV is consistent with the value for P in the PO_4^{3+} [38, 39]. Recently, it is reported that phosphorus can be doped into the bulk of hematite uniformly by soaking FeOOH into the Na_2HPO_4 solution, following by annealing at 650 or 750 ^oC [40]. In our study, based on the XPS profiles, the molar ratios of P/Fe in sample Fe_2O_3-Ag-P is calculated to be 0.61, which is much higher than the ratio determined by EDS (0.01). The sample depth can be analyzed by XPS is less than 10 nm, so the $r_{P/Fe}$ detected by XPS is only the element atomic ratio on the exterior surface of sample Fe_2O_3-Ag-P. However, for EDS, the depth detected is more than 100 nm, which means that the $r_{P/Fe}$ ratio determined by EDS is the element atomic ratio in the bulk of the sample Fe_2O_3-Ag-P. This further proves that the phosphate groups were mainly adsorbed on the surface, not doped in the bulk of the sample.

3.3 Photoelectrochemical performances

The improvement in PEC activity induced by Ag doping and phosphate adsorption was further verified by investigating the incident photon-to-current efficiency (IPCE) of sample Fe_2O_3-Ag_3PO_4-5 and Fe_2O_3-Ag-P at 1.23 V_{RHE}. As shown in Fig.11, the hematite films mediated by Ag_3PO_4 both showed higher IPCE than that of bare Fe_2O_3. The IPCE values of 18.1 % and 23.8% were obtained at 400 nm for Fe_2O_3-Ag_3PO_4-5 and Fe_2O_3-Ag-P in 1.0 M NaOH aqueous solution at 1.23 V_{RHE}, respectively. The enhancement in IPCE compared with the bare Fe_2O_3 is in agreement with the *J-V* results. As moving to long wavelengths, the IPCE decreased sharply and substantially to nearly zero above 590 nm.

Then PEC measurements of the hematite films mediated by Ag_3PO_4 and bare Fe_2O_3 were conducted in the presence of H_2O_2 to investigate the charge separation and hole injection yields, which are calculated using eq. (3) and (4).

$$\eta_{\text{charge separation}} = J_{H2O2}/J_{\text{absorbed}} \quad (3)$$

$$\eta_{\text{charge injection}} = J_{H2O}/J_{H2O2} \quad (4)$$

Where, $J_{absorbed}$ is the photocurrent obtained by integrating the absorption spectra, and was calculated to be 9.8, 9.2, and 10.3 mA/cm^2 for Fe_2O_3-Ag-P, Fe_2O_3-Ag_3PO_4-5, and bare Fe_2O_3, respectively. The values of the J_{H2O} photocurrent and J_{H2O2} photocurrent are shown in supporting information (Fig.S4). With these values, the charge separation and hole injection yields were obtained according to eq. (1) and (2), and the results were shown in Fig. 12. As potentials increase, charge separation yields of the Fe_2O_3-Ag-P and Fe_2O_3-Ag_3PO_4-5 gradually increase, and reach 10.1% and 8.5%, respectively, at a potential of 1.23 V_{RHE}. But the bare Fe_2O_3 electrode has little change in the charge separation yield with increasing potential. Higher charge separation yields for the hematite electrodes mediated by Ag_3PO_4 may be due to the nanocube structure, facilitating charge transfer and minimizing bulk charge recombination.

The hole injection yields of the three electrodes increased with the potential. Compared to bare Fe_2O_3, relatively steeper rise was observed for Fe_2O_3-Ag-P and Fe_2O_3-Ag_3PO_4-5 electrodes, and hole injection yields of 93.8% and 87.9% were obtained at a potential of 1.23 V_{RHE}, respectively. Their high hole injection yields probably benefits from the doped Ag, which was considered as promoter of increasing the charge carrier density and accelerating the surface oxidative reaction kinetics [11]. In addition, a negative electrostatic field formed by phosphate ions on the Fe_2O_3 surface would accelerate extraction of photoexcited holes to the electrode surface. The two factors results in more efficient hole injection. Hematite films mediated by Ag_3PO_4, especially by *in-situ* formed Ag_3PO_4, showed a hole injection yield as high as 93.8 % at 1.23 V_{RHE}, suggesting that the photocurrent of the electrode at 1.23 V_{RHE} is mainly limited by the charge separation efficiency because of the efficient hole injection. The low charge separation yield can be ascribed to serious bulk recombination resulted from extremely short hole diffusion length (2–4 nm). As shown in Fig. 12a, an alternative nanocube structure is beneficial to minimize bulk charge recombination in α-Fe_2O_3 film.

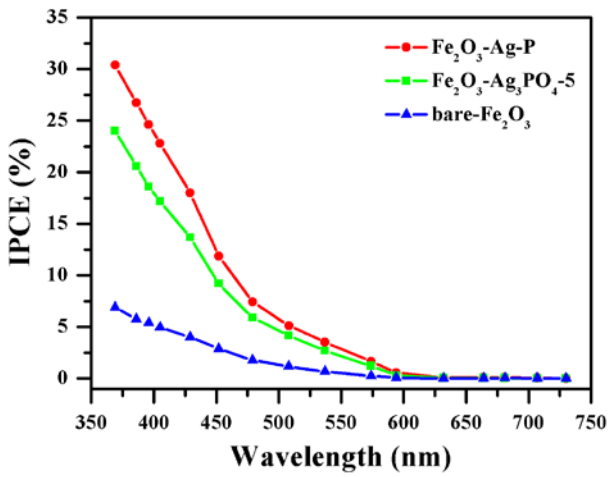

Fig. 11 IPCE spectra of the Fe_2O_3-Ag-P, Fe_2O_3-Ag_3PO_4-5, and bare Fe_2O_3.

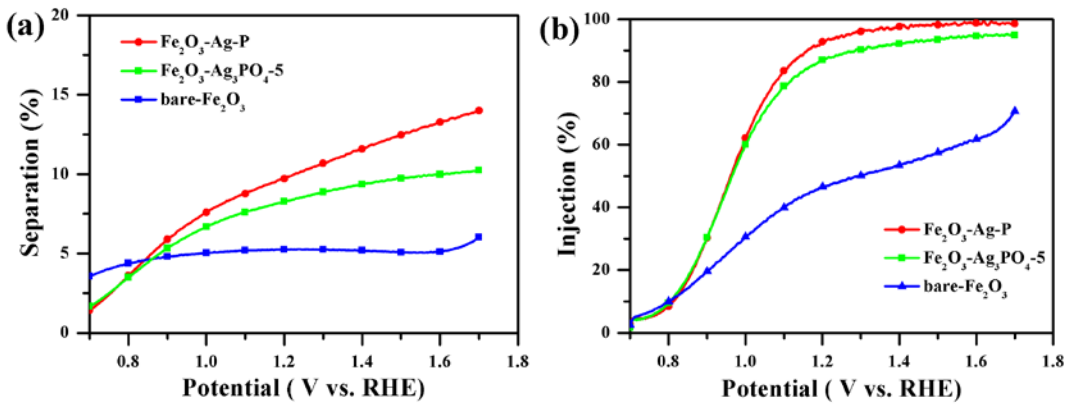

Fig. 12 (a) Yields of charge separation of Fe_2O_3-Ag-P, Fe_2O_3-Ag_3PO_4-5, and bare Fe_2O_3; (b) Yields of charge injection from the surface of electrodes to electrolyte

Conclusions

We have synthesized nanocube structured α-Fe_2O_3 thin film on FTO substrate from FeOOH nanorod arrays mediated by Ag_3PO_4. Ag-doped and phosphate ions coated α-Fe_2O_3 nanocubes films (Fe_2O_3-Ag_3PO_4-5) were synthesized through spin coating Ag_3PO_4 powder on FeOOH film followed by high temperature annealing. A high photocurrent of 0.70 mA cm^{-2} was observed for prepared hematite film photoanode compared to bare Fe_2O_3. The photocurrent improvement is attributed to three factors: 1) the nanocube structure, which facilitates charge transfer and minimizing bulk charge recombination; 2) the doped Ag, increasing the charge carrier density and accelerating the surface oxidative reaction kinetics; 3) the absorbed phosphate ions, establishing a

negative electrostatic field on hematite surface and promoting hole transfer. The photocurrent can be further improved to 0.98 mA cm^{-2} by the *in-situ* formed Ag_3PO_4 in the solution of $AgNO_3$ and KH_2PO_4. The well-distributed nano Ag_3PO_4 on the FeOOH film resulted in uniform α-Fe_2O_3 nanocubes for effective PEC performances. These findings provide a facile method combining the morphology control and surface modification together for preparation of nanostructured photoelectrodes for efficient solar water splitting.

Acknowledgements

We gratefully acknowledge financial support from the National Natural Science Foundation of China (21576215, 21503147) and Tianjin Natural Science Foundation (13JCZDJC32400)

1. Sivula, K., F. Le Formal, and M. Graetzel, *Solar water splitting: progress using hematite (alpha-Fe_2O_3) photoelectrodes.* Chemsuschem, 2011. **4**(4): p. 432-449.
2. Bak, C.H., et al., *Efficient photoelectrochemical water splitting of nanostructured hematite on a three-dimensional nanoporous metal electrode.* J. Mater. Chem. A, 2014. **2**(41): p. 17249-17252.
3. Wheeler, D.A., et al., *Nanostructured hematite: synthesis, characterization, charge carrier dynamics, and photoelectrochemical properties.* Energy & Environmental Science, 2012. **5**(5): p. 6682-6702.
4. Bora, D.K., A. Braun, and E.C. Constable, *"In rust we trust". Hematite - the prospective inorganic backbone for artificial photosynthesis.* Energy & Environmental Science, 2013. **6**(2): p. 407-425.
5. Brillet, J., et al., *Examining architectures of photoanode–photovoltaic tandem cells for solar water splitting.* Journal of Materials Research, 2010. **25**(01): p. 17-24.
6. Kim, J.Y., et al., *Single-crystalline, wormlike hematite photoanodes for efficient solar water splitting.* Sci Rep, 2013. **3**: p. 2681.
7. Sivula, K., F. Le Formal, and M. Graetzel, *WO_3-Fe_2O_3 photoanodes for water splitting: a host scaffold, guest absorber approach.* Chemistry of Materials, 2009. **21**(13): p. 2862-2867.
8. Cherepy, N.J., et al., *Ultrafast studies of photoexcited electron dynamics in gamma- and alpha-Fe_2O_3 semiconductor nanoparticles.* Journal of Physical Chemistry B, 1998. **102**(5): p. 770-776.
9. Tilley, S.D., et al., *Light-induced water splitting with hematite: improved nanostructure and iridium oxide catalysis.* Angewandte Chemie, 2010. **122**(36): p. 6549-6552.
10. Liu, R., et al., *Enhanced photoelectrochemical water-splitting performance of semiconductors by surface passivation layers.* Energy & Environmental Science, 2014. **7**(8): p. 2504-2517.
11. Shen, S., et al., *Surface engineered doping of hematite nanorod arrays for improved photoelectrochemical water splitting.* Sci Rep, 2014. **4**: p. 6627.

12. Ling, Y., et al., *Sn-Doped Hematite Nanostructures for Photoelectrochemical Water Splitting.* Nano Letters, 2011. **11**(5): p. 2119-2125.
13. Kay, A., I. Cesar, and M. Grätzel, *New benchmark for water photooxidation by nanostructured α-Fe_2O_3 films.* Journal of the American Chemical Society, 2006. **128**(49): p. 15714-15721.
14. Cesar, I., et al., *Influence of Feature Size, Film Thickness, and Silicon Doping on the Performance of Nanostructured Hematite Photoanodes for Solar Water Splitting.* Journal of Physical Chemistry C, 2009. **113**(2): p. 772-782.
15. Lin, Y., et al., *Nanonet-based hematite heteronanostructures for efficient solar water splitting.* Journal of the American Chemical Society, 2011. **133**(8): p. 2398-2401.
16. Goncalves, R.H., B.H.R. Lima, and E.R. Leite, *Magnetite Colloidal Nanocrystals: A Facile Pathway To Prepare Mesoporous Hematite Thin Films for Photoelectrochemical Water Splitting.* Journal of the American Chemical Society, 2011. **133**(15): p. 6012-6019.
17. Le Formal, F., et al., *Passivating surface states on water splitting hematite photoanodes with alumina overlayers.* Chemical Science, 2011. **2**(4): p. 737-743.
18. Hisatomi, T., et al., *Cathodic shift in onset potential of solar oxygen evolution on hematite by 13-group oxide overlayers.* Energy and Environmental Science, 2011. **4**(7): p. 2512-2515.
19. Zhong, D.K., et al., *Photo-assisted electrodeposition of cobalt–phosphate (Co–Pi) catalyst on hematite photoanodes for solar water oxidation.* Energy & Environmental Science, 2011. **4**(5): p. 1759.
20. Zhong, D.K. and D.R. Gamelin, *Photoelectrochemical Water Oxidation by Cobalt Catalyst ("Co−Pi")/α-Fe2O3 Composite Photoanodes: Oxygen Evolution and Resolution of a Kinetic Bottleneck.* Journal of the American Chemical Society, 2010. **132**(12): p. 4202-4207.
21. Young, K.M. and T.W. Hamann, *Enhanced photocatalytic water oxidation efficiency with $Ni(OH)_2$ catalysts deposited on alpha-Fe_2O_3 via ALD.* Chem Commun (Camb), 2014. **50**(63): p. 8727-30.
22. Bora, D.K., et al., *Hematite-NiO/alpha-Ni(OH)(2) heterostructure photoanodes with high electrocatalytic current density and charge storage capacity.* Physical Chemistry Chemical Physics, 2013. **15**(30): p. 12648-12659.
23. Zeng, Q., et al., *A novel in situ preparation method for nanostructured alpha-Fe2O3 films from electrodeposited Fe films for efficient photoelectrocatalytic water splitting and the degradation of organic pollutants.* Journal of Materials Chemistry A, 2015. **3**(8): p. 4345-4353.
24. Wang, Z., et al., *Synergetic Effect of Conjugated Ni(OH)(2)/IrO2 Cocatalyst on Titanium-Doped Hematite Photoanode for Solar Water Splitting.* Journal of Physical Chemistry C, 2015. **119**(34): p. 19607-19612.
25. Shen, S., et al., *Surface Tuning for Promoted Charge Transfer in Hematite Nanorod Arrays as Water-Splitting Photoanodes.* Nano Research, 2012. **5**(5): p. 327-336.
26. Shen, S., et al., *Effect of Cr doping on the photoelectrochemical performance of hematite nanorod photoanodes.* Nano Energy, 2012. **1**(5): p. 732-741.
27. Xi, L.F., et al., *A novel strategy for surface treatment on hematite photoanode for efficient water oxidation.* Chemical Science, 2013. **4**(1): p. 164-169.
28. Cheng, W., et al., *Ni-Doped Overlayer Hematite Nanotube: A Highly Photoactive Architecture for Utilization of Visible Light.* Journal of Physical Chemistry C, 2012. **116**(45): p. 24060-24067.
29. Kim, J.Y., et al., *A stable and efficient hematite photoanode in a neutral electrolyte for solar water splitting: towards stability engineering.* Advanced Energy Materials, 2014. **4**(13): p.

14004761-14004767.

30. Liu, K., et al., *Nanocube-based hematite photoanode produced in the presence of Na_2HPO_4 for efficient solar water splitting.* Journal of Power Sources, 2015. **283**(0): p. 381-388.
31. Ge, M., et al., *Sunlight-Assisted Degradation of Dye Pollutants in Ag3PO4 Suspension.* Industrial & Engineering Chemistry Research, 2012. **51**(14): p. 5167-5173.
32. Vayssieres, L., et al., *Controlled aqueous chemical growth of oriented three-dimensional crystalline nanorod arrays: application to iron(III) oxides.* Chemistry of Materials, 2001. **13**(2): p. 233-235.
33. Morales, M.P., T. Gonzalezcarreno, and C.J. Serna, *The formation of alpha-Fe_2O_3 monodispersed particles in solution.* Journal of Materials Research, 1992. **7**(9): p. 2538-2545.
34. Guo, S.-y., et al., *Self-assembly synthesis of precious-metal-free 3D ZnO nano/micro spheres with excellent photocatalytic hydrogen production from solar water splitting.* Journal of Power Sources, 2015. **293**: p. 17-22.
35. Liu, J., et al., *Highly oriented Ge-doped hematite nanosheet arrays for photoelectrochemical water oxidation.* Nano Energy, 2014. **9**: p. 282-290.
36. Schon, G., *Esca studies of Ag, Ag_2O and AgO.* Acta Chemica Scandinavica, 1973. **27**(7): p. 2623-2633.
37. Bai, S., et al., *Assembly of Ag3PO4 nanocrystals on graphene-based nanosheets with enhanced photocatalytic performance.* J Colloid Interface Sci, 2013. **405**: p. 1-9.
38. Castro, L., et al., *The Spin-Polarized Electronic Structure of LiFePO4 and FePO4 Evidenced by in-Lab XPS.* The Journal of Physical Chemistry C, 2010. **114**(41): p. 17995-18000.
39. J. F. Moulder, W.F.S., P. E. Sobol and K. D. Bomben, *Handbook of X-ray Photoelectron Spectroscopy*. 1992, Eden Prairie,: Perkin-Elmer Corporation.
40. Yuchao Zhang, S.J., Wenjing Song,a Peng Zhou,, *Nonmetal P-doped hematite photoanode with enhanced electron mobility and high water oxidation activity.*